



Quantifying spin relaxation in mesoscopic Cu channels via a multitude of nonlocal spin valves

Yunjiao Cai ¹, Chuan Qin,^{1,*} Fatih Kandaz,^{1,†} Xingyu Shen,¹ Chao Zhou,² Mengwen Jia,²
Yongming Luo,^{2,3} Yizheng Wu,² and Yi Ji^{1,‡}

¹*Department of Physics and Astronomy, University of Delaware, Newark, Delaware 19716, USA*

²*Department of Physics, State Key Laboratory of Surface Physics, Fudan University, Shanghai 200433, People's Republic of China*

³*Center for Integrated Spintronic Devices, Hangzhou Dianzi University, Hangzhou, Zhejiang 310018, People's Republic of China*

 (Received 17 April 2019; revised manuscript received 27 August 2019; published 14 October 2019)

We fabricate a large number (>100) of nonlocal spin valves with mesoscopic Cu channels. A systematic method is used to extract Cu resistivity ρ_{Cu} and spin relaxation length λ_{Cu} from each given structure. A relationship between λ_{Cu} and ρ_{Cu} is established over a broad range of ρ_{Cu} (from 0.7 to $>10 \mu\Omega \text{ cm}$) with >200 data points obtained at 10 and 295 K. Quantitative analysis of the relationship indicates that the spin relaxation can be described by the Elliott-Yafet model with a low spin-flip probability of $(1.9 \pm 0.2) \times 10^{-4}$ for bulk scattering and a higher probability of $(1.6 \pm 0.2) \times 10^{-3}$ for surface scattering. Encouraging large values of λ_{Cu} ($\sim 2.0 \mu\text{m}$ at 10 K and $\sim 700 \text{ nm}$ at 295 K) are achieved experimentally in structures with low ρ_{Cu} values ($\leq 1.0 \mu\Omega \text{ cm}$ at 10 K and $\leq 4.0 \mu\Omega \text{ cm}$ at 295 K).

DOI: [10.1103/PhysRevB.100.144419](https://doi.org/10.1103/PhysRevB.100.144419)

I. INTRODUCTION

Spin-relaxation length λ is an important materials parameter for spintronics. A long spin-relaxation length is desired for materials to maintain a spin current or spin accumulation over distance. The relationship between the λ and the resistivity ρ is of significance as well, because it reflects the mechanism of spin relaxation. There are two prevailing spin-relaxation mechanisms in the literature: Elliott-Yafet (EY) model [1,2] and Dyakonov-Perel (DP) model [3]. In the EY model, the spin relaxation occurs with a finite probability (spin-flip probability α) at each instance of momentum relaxation. For a fixed value of α , the spin-relaxation time τ_s is proportional to the momentum relaxation time τ_e , or equivalently λ is inversely proportional to ρ . In the DP model, however, the spin relaxation occurs through continuous precession (dephasing) of spins under a momentum-dependent spin-orbital field between momentum relaxation events. A momentum relaxation event randomizes the direction of the spin-orbital field and actually enhances τ_s . Therefore, the DP model predicts that τ_s is inversely proportional to τ_e or equivalently λ is independent of ρ .

Spin-relaxation length λ is not a directly measurable quantity and its determination often requires quantitative analysis based on a series of samples and measurements. The spin-relaxation length λ of nonmagnetic materials, if sufficiently large ($\lambda > 10^2 \text{ nm}$), can be measured by using the nonlocal spin-valve (NLSV) structures [4,5]. These are mesoscopic lateral structures that consist of a nonmagnetic spin-transport channel, a magnetic spin injector (F_1), and a magnetic spin

detector (F_2). The nonlocal spin signal is typically measured as a function of the length of channel L between the F_1 and F_2 . Quantitative analysis of the decaying trend of the spin signal yields an average λ for the channel and an average spin polarization P for F_1 and F_2 . [5–10]

While it is known that λ depends sensitively on the microstructures and purity of the nonmagnetic metallic channel, an explicit investigation of the possible range of λ and its correlation with resistivity ρ is lacking even for common nonmagnetic materials such as Cu. In this work, we use an exceptionally large number (>100) of NLSVs to explicitly explore the relationship between λ_{Cu} and ρ_{Cu} for mesoscopic Cu channels. The thickness and width of the Cu channels vary between 100 and 300 nm. The variation of measured ρ_{Cu} is more than a factor of 5 at 10 K and exceeds a factor of 12 if incorporating data for both 10 and 295 K. A systematic method is used to extract a spin-relaxation length λ_{Cu} from the measured ΔR_s and ρ_{Cu} of a given NLSV (at 10 or/and 295 K), and thereby establishing a plot of λ_{Cu} versus ρ_{Cu} over a substantial range of ρ_{Cu} .

Encouraging large values ($\sim 2 \mu\text{m}$ at 10 K) of λ_{Cu} can be achieved in some NLSVs in which the ρ_{Cu} is $< 1.0 \mu\Omega \text{ cm}$ at 10 K and the residual resistivity ratio (ratio of the 295 K resistivity to the 10 K resistivity) is large (e.g., ~ 5). Quantitative analysis of the λ_{Cu} versus ρ_{Cu} relationship reveals that the Elliott-Yafet model is a valid description of the spin-relaxation mechanism. However, there is a sharp contrast between a low spin-flip probability for the bulk scattering and a much higher spin-flip probability for surface scattering events. This is consistent with recent experiments that suggest a substantial contribution of spin-orbit effects on the surfaces of mesoscopic Cu channels [11].

II. EXPERIMENTAL METHODS

The NLSV structures are fabricated by using electron-beam lithography followed by electron-beam evaporation. Two layers of electron-beam resists, polymethyl methacrylate

*Present address: Western Digital Corporation, 44100, Osgood Road, Fremont, California 94539, USA.

†Present address: Department of Physics, Gebze Technical University, Gebze 41400, Turkey.

‡yji@udel.edu

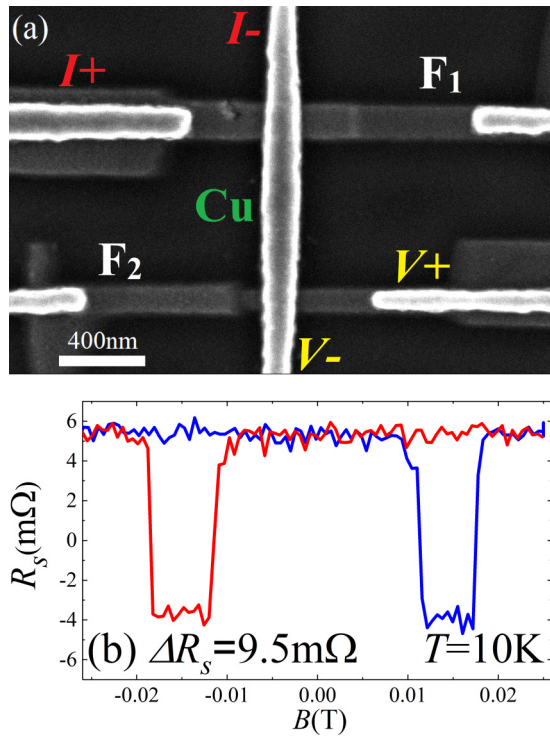


FIG. 1. (a) SEM image for a NLSV device with a mesoscopic Cu channel. (b) R_s versus B curves at 10 K for a NLSV. The thickness and width of Cu channel are 200 and 240 nm, respectively. The channel length between F_1 and F_2 is $L = 900$ nm.

on the top and polydimethylglutarimide at the bottom, are coated on a silicon substrate covered by 200 nm SiN. Mesoscopic suspended resist shadow masks are formed in the resist layers after electron-beam lithography and development. The NLSVs are made by evaporating materials from various incident angles through the masks in a single deposition run [12–14]. The scanning electron microscope image of a finished NLSV is shown in Fig. 1(a). The spin injector (F_1) and spin detector (F_2) are made of permalloy (Py, NiFe alloy) and the nonmagnetic channel is made of Cu. A 3-nm layer of AlO_x is directly evaporated between F_1 (or F_2) and Cu to maintain a substantial polarization P . The resistance of such an AlO_x junction with $100 \times 100\text{-nm}^2$ size is typically between 1 and 20 Ω , much lower than that of a uniform tunnel junction.

TABLE I. Relevant parameters of ten substrates used in this work, including Cu channel thickness, average width of Cu channels, number of devices measured at 10 K, fitted P_e (effective spin polarization) at 10 K, number of devices measured at 295 K, and fitted P_e at 295 K.

Substrate No.	Cu thk (nm)	avg Cu width (nm)	No. of dev at 10 K	P_e at 10 K (%)	No. of dev at 295 K	P_e at 295 K (%)
68-8	110	208	24	12.4 ± 2.9	NA	NA
57-7	110	125	20	15.7 ± 0.9	15	7.4 ± 1.3
58-7	110	131	11	19.3 ± 2.5	NA	NA
61-4	130	102	8	15.7 ± 2.8	NA	NA
64-2	110	213	9	17.4 ± 7.0	NA	NA
67-6	110	157	7	20.1 ± 3.1	16	11.2 ± 1.6
68-7	200	176	10	16.6 ± 2.3	NA	NA
70-0	250	226	23	13.1 ± 2.8	23	7.7 ± 1.9
70-1	110	197	NA	NA	6	13.1 ± 3.6
70-4	200	180	16	22.2 ± 2.9	14	12.1 ± 1.5

Up to 25 NLSVs are fabricated on each sample substrate through identical processing conditions. Therefore, a given component (F_1 , F_2 , Cu channel, or AlO_x barrier) of NLSVs acquires identical thickness and consistent quality on the same substrate. On a given substrate, while the distance L between F_1 and F_2 is varied for NLSV devices, the respective widths of F_1 and F_2 remain nominally the same. The width of Cu channels on a given substrate is either designed to be nominally the same or varied intentionally (by less than a factor of 2) to induce additional variation in the Cu resistivity ρ_{Cu} . This work involves a total of 10 substrates, and the number of NLSVs successfully measured from each substrate is between 6 and 25. Altogether 128 devices are measured at 10 K and 74 devices are measured at 295 K, giving rise to 202 data points. The overall range of the thickness and width of the Cu channels is between 100 and 300 nm. The range of L is between 300 and 1500 nm. The widths of F_1 and F_2 are mostly between 120 and 200 nm. Relevant parameters (dimensions and number of devices, etc.) of all substrates are given in Table I.

For measurement, an alternating current (ac) of $I_e = 0.1$ mA with low frequency (346 Hz) is applied between F_1 ($I+$) and the upper end of the Cu channel ($I-$), as shown in Fig. 1(a). The nonlocal voltage V_{nl} is measured by lock-in method between F_2 ($V+$) and the lower end of the Cu channel ($V-$). The nonlocal resistance $R_s = V_{\text{nl}}/I_e$ at 10 K as a function of magnetic field B , applied parallel to F_1 and F_2 stripes, is shown in Fig. 1(b) for a NLSV. The thickness and width of the Cu channel for this NLSV are 200 and 240 nm, respectively, and the channel length between F_1 and F_2 is $L = 900$ nm. The widths of F_1 and F_2 for a given NLSV are designed with a small difference to achieve different switching fields. The high states and low states of R_s correspond to the parallel and antiparallel alignments of F_1 and F_2 spins, respectively. The spin signal, defined as the difference in R_s between two states, is $\Delta R_s = 9.5$ m Ω . This is a substantial value considering the long channel length and large Cu cross section.

III. ESTABLISHING λ_{Cu} VERSUS ρ_{Cu} RELATIONSHIP

For NLSV with oxide interfaces, the spin signal is described by the formula [15,16]

$$\Delta R_s = \frac{P_e^2 \rho_{\text{Cu}} \lambda_{\text{Cu}}}{A_{\text{Cu}}} e^{-(L/\lambda_{\text{Cu}})}, \quad (1)$$

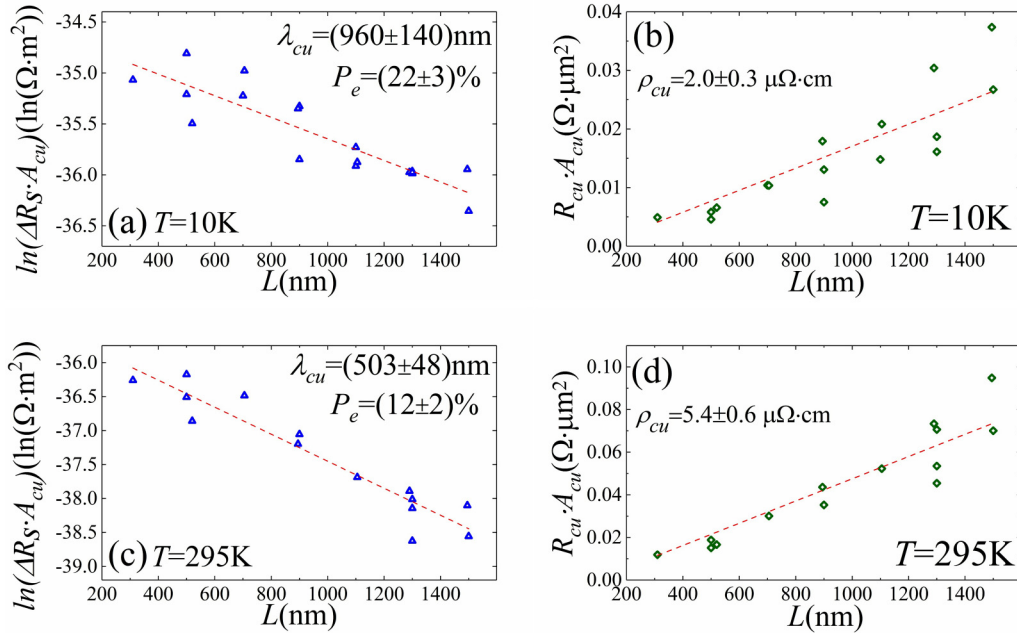


FIG. 2. (a) Plot of $\ln(\Delta R_s A_{Cu})$ versus L and (b) plot of $R_{Cu} A_{Cu}$ versus L at 10 K for 16 NLSVs on substrate No. 70-4. The values of ΔR_s are between 4.5 and 17.4 m Ω . The linear fits to the data are shown as the dashed lines and the fitting parameters yield $\rho_{Cu} = (2.0 \pm 0.3) \mu\Omega \text{ cm}$, $P_e = (22 \pm 3)\%$, and $\lambda_{Cu} = (960 \pm 140) \text{ nm}$. (c) Plot of $\ln(\Delta R_s A_{Cu})$ versus L and (b) plot of $R_{Cu} A_{Cu}$ versus L at 295 K for NLSVs on substrate No. 70-4. The linear fits to the data are shown as the dashed lines and the fitting parameters yield $\rho_{Cu} = (5.4 \pm 0.6) \mu\Omega \text{ cm}$, $P_e = (12 \pm 2)\%$, and $\lambda_{Cu} = (503 \pm 48) \text{ nm}$. The Cu thickness is 200 nm and the Cu width varies between 120 and 250 nm.

where P_e is the effective spin polarization for F_1 and F_2 , A_{Cu} is the cross-sectional area of the Cu channel, and L is the center-to-center distance between F_1 and F_2 along the channel. For NLSVs with F_1 and F_2 made from the same materials with similar dimensions, it is common to assume that they have the same P_e . To take into account the Cu width variations, either by design or because of lithography inconsistency, we carefully measure the exact widths by scanning electron microscopy (SEM) for each NLSV and rewrite Eq. (1) into

$$\ln(\Delta R_s A_{Cu}) = -\frac{L}{\lambda_{Cu}} + \ln(P_e^2 \rho_{Cu} \lambda_{Cu}). \quad (2)$$

When $\ln(\Delta R_s A_{Cu})$ is plotted as a function of L for NLSVs on a given substrate and fitted by a straight line, the slope ($-1/\lambda_{Cu}$) of the line allows for an estimate of average λ_{Cu} assuming that all NLSVs have the same λ_{Cu} , P_e , and ρ_{Cu} . Figure 2(a) shows such a plot at 10 K for 16 NLSVs on substrate No. 70-4, for which the Cu thickness is 200 nm and Cu width is between 100 and 250 nm. The spin signals are between 4.5 and 17.4 m Ω . A linear fit (dashed line) generates the fitted value of $\lambda_{Cu} = (960 \pm 140) \text{ nm}$.

Evaluation of P_e requires the value of ρ_{Cu} . The resistance of the Cu channel, $R_{Cu} = \rho_{Cu} \frac{L}{A_{Cu}}$, is measured for each NLSV by sending in a current through the Cu channel and measuring the voltage on the F_1 and F_2 stripes. The $R_{Cu} A_{Cu}$ versus L relationship should be a straight line passing the origin and its slope is the average resistivity, because $R_{Cu} A_{Cu} = \rho_{Cu} L$. Figure 2(b) shows the plot of the $R_{Cu} A_{Cu}$ versus L at 10 K for NLSVs on substrate A. However, the straight line that fits the data best does not pass the origin. This is possible if the effective voltage detection points on the F_1 or F_2 stripes

deviate from their geometrical centers. Therefore, we allow a nonzero horizontal intercept that is temperature independent and no more than the sum of the half widths of F_1 and F_2 . In this manner, a horizontal intercept of 86 nm is used for both 10 and 295 K for substrate A. The average resistivity (slope) is determined to be $\rho_{Cu} = (2.0 \pm 0.3) \mu\Omega \text{ cm}$ at 10 K. Afterwards, average effective spin polarization $P_e = 0.22 \pm 0.03$ is determined from the vertical intercept of the fitted line for $\ln(\Delta R_s A_{Cu})$ versus L in Fig. 2(a).

The values of $\lambda_{Cu} = (960 \pm 140) \text{ nm}$, $\rho_{Cu} = (2.0 \pm 0.3) \mu\Omega \text{ cm}$, and $P_e = 0.22 \pm 0.03$ should be viewed as the average values of spin-relaxation length, resistivity, and effective spin polarization at 10 K for the NLSV devices on sample substrate No. 70-4. Figures 2(c) and 2(d) show plots of $\ln(\Delta R_s A_{Cu})$ versus L and the $R_{Cu} A_{Cu}$ versus L for substrate No. 70-4 at 295 K, respectively. Using a similar approach, we determine $\lambda_{Cu} = (503 \pm 48) \text{ nm}$, $\rho_{Cu} = (5.4 \pm 0.6) \mu\Omega \text{ cm}$, and $P_e = 0.12 \pm 0.02$ at 295 K. The scattering of the experimental data around the fitted lines in Figs. 2(a) through 2(d) indicates variations in λ_{Cu} , ρ_{Cu} , or P_e among NLSVs even on the same substrate. In the following, we will extract values of λ_{Cu} and ρ_{Cu} from each NLSV and establish a correlation between λ_{Cu} and ρ_{Cu} , while assuming that P_e is the same for all NLSVs on a given substrate.

The value of ρ_{Cu} for a given NLSV is calculated from the measured resistance by using $R_{Cu} = \rho_{Cu} \frac{L}{A_{Cu}}$ with the caution that the L value should be adjusted by the horizontal intercept of the fitted line in the $R_{Cu} A_{Cu}$ versus L plot. The λ_{Cu} is calculated from the ΔR_s and ρ_{Cu} of a given NLSV and the fitted P_e of the substrate by using Eq. (1). Figures 3(a) and 3(b) shows the plot of λ_{Cu} versus ρ_{Cu} for NLSVs on substrate No. 70-4 at 10 and 295 K, respectively. The error bars are

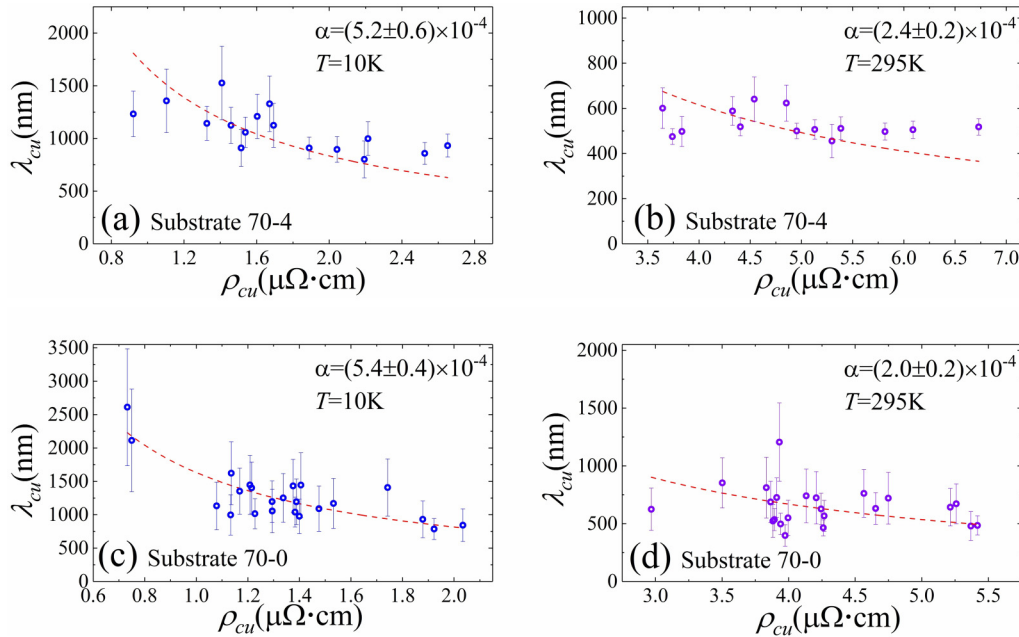


FIG. 3. Plots of λ_{Cu} versus ρ_{Cu} for (a) substrate No. 70-4 at 10 K, (b) substrate No. 70-4 at 295 K, (c) substrate No. 70-0 at 10 K, and (d) substrate No. 70-0 at 295 K. The dashed lines are fits by Eq. (3) and the fitted spin-flip probabilities α are shown in each panel.

calculated from the standard deviation of fitted P_e and the estimated errors of ρ_{Cu} . In Fig. 3(a), the ρ_{Cu} ranges between 0.9 and 2.7 $\mu\Omega$ cm and there is a decreasing trend in the plot of λ_{Cu} versus ρ_{Cu} despite the scattering of data points. In Fig. 3(b), the ρ_{Cu} ranges between 3.7 and 6.7 $\mu\Omega$ cm and λ_{Cu} appears to be independent of the ρ_{Cu} . Figures 3(c) and 3(d) show the λ_{Cu} versus ρ_{Cu} plots for 23 NLSVs on substrate No. 70-0 at 10 and 295 K, respectively. The Cu channels on substrate No. 70-0 have a thickness of 250 nm and widths between 155 and 290 nm. Similarly, there is a broader range of ρ_{Cu} and a more obvious trend of decreasing λ_{Cu} with increasing ρ_{Cu} for 10 K than for 295 K.

It is interesting to note that ρ_{Cu} varies from device to device on any given substrate despite the identical processing conditions. This highlights the sensitive dependence of ρ_{Cu} on the microstructures and dimensions of the Cu channels. A thinner and narrower Cu channel would result in more surface scattering and higher ρ_{Cu} . Even when the dimensions are the same for all devices on a substrate, variation of ρ_{Cu} is still unavoidable because of the microstructure variation between devices.

The Elliott-Yafet model predicts an inversely proportional relationship between λ_{Cu} and ρ_{Cu} with the assumption of a constant spin-flip probability α . Note that spin-flip probability α is the ratio of spin-relaxation rate $1/\tau_s$ (occurrences of spin relaxation per unit time) to the momentum scattering rate $1/\tau_e$ (occurrences of momentum relaxation per unit time), or $1/\tau_s = \alpha/\tau_e$. The momentum scattering time τ_e is related to ρ_{Cu} : $\tau_e = m/(\rho_{Cu}ne^2)$, where m and e are the mass and charge for an electron and $n = 8.47 \times 10^{28} \text{m}^{-3}$ is the electron density in Cu [17]. The spin-relaxation time τ_s is linked to λ_{Cu} : $\tau_s = \lambda_{Cu}^2/D$, where $D = \frac{1}{3}v_F^2\tau_e$ is the diffusion constant for degenerate electrons in metal [18,19] and $v_F = 1.57 \times 10^6$ m/s is the Fermi velocity for Cu [17]. Summarizing these

formulas, we have

$$\lambda_{Cu} = \frac{1}{\rho_{Cu}} \left(\frac{mv_F}{ne^2\sqrt{3\alpha}} \right). \quad (3)$$

We attempt to fit the λ_{Cu} versus ρ_{Cu} plots by using Eq. (3), and the dashed lines in Figs. 3(a) through 3(d) are the best fits. The fitted values of α are $(5.2 \pm 0.6) \times 10^{-4}$ (No. 70-4 at 10 K), $(2.4 \pm 0.2) \times 10^{-4}$ (No. 70-4 at 295 K), $(5.4 \pm 0.4) \times 10^{-4}$ (No. 70-0 at 10 K), and $(2.0 \pm 0.2) \times 10^{-4}$ (No. 70-0 at 295 K) for Figs. 3(a)–3(d), respectively. The values are quite consistent between substrates No. 70-4 and No. 70-0 for a given temperature, reaffirming the validity of the methods used to extract ρ_{Cu} and λ_{Cu} . The difference in α values between 10 and 295 K is interesting and will be addressed later. The standard deviations for these α values are reasonably small, even though the quality of fitting is less than satisfactory for some plots in Fig. 3. We note that the α values can be directly calculated from the λ_{Cu} and ρ_{Cu} of any given NLSV by using Eq. (3) without fitting. Therefore, the α values are influenced more by the average values of λ_{Cu} and ρ_{Cu} for a given set of NLSVs than by the precise relationship between λ_{Cu} and ρ_{Cu} .

For 10 K in Figs. 3(a) and 3(c), the fitted curves reproduce qualitatively the decreasing trend in the λ_{Cu} versus ρ_{Cu} plot, indicating that the spin relaxation can be described by the Elliott-Yafet model. For 295 K in Figs. 3(b) and 3(d), fitted curves are relatively flat with smaller values of α . This leaves us two possibilities in regard to the spin relaxation at 295 K: (i) The actual λ_{Cu} values decay very slowly as a function of ρ_{Cu} because of small α values, but the scattering of experimental λ_{Cu} values and limited range of ρ_{Cu} result in an apparent flat feature; (ii) the spin-relaxation mechanism is more of the DP type, which predicts that λ_{Cu} is independent of ρ_{Cu} . Note that the variations of ρ_{Cu} are quite limited and

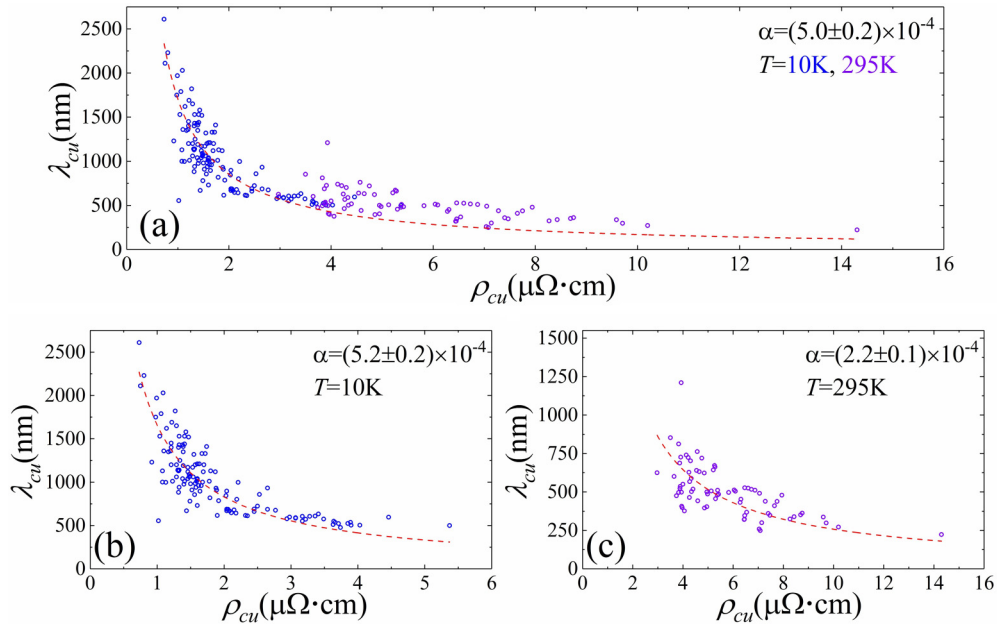


FIG. 4. Plots of λ_{cu} versus ρ_{cu} for (a) all NLSVs at both 10 K (blue) and 295 K (purple), (b) NLSVs at 10 K, and (c) NLSVs at 295 K. The dashed lines are fits by Eq. (3) and the fitted spin-flip probabilities α are shown in each panel.

less than a factor of 2 at 295 K in Figs. 3(b) or 3(d). Such limited ranges of ρ_{Cu} make it difficult to be conclusive. In the remainder of this section and the following sections, we will show that the λ_{Cu} versus ρ_{Cu} curve over a broad range of ρ_{Cu} can be fully described by the EY model.

In the following, we will show that the λ_{Cu} versus ρ_{Cu} relationship can be better established by using a large number of data points over a broader range of ρ_{Cu} . We combine the available λ_{Cu} versus ρ_{Cu} data from all ten sample substrates listed in Table I. Figure 4(a) is a plot that includes all 202 data points for both 10 and 295 K. The ρ_{Cu} value varies strikingly by more than one order of magnitude from 0.7 to $>10 \mu\Omega \text{cm}$. Error bars are not included in this plot, because the spread of the data points along the λ_{Cu} axis around a specific ρ_{Cu} is comparable to the errors of λ_{Cu} . Therefore, we regard the spread of the data points as a representation of the uncertainties. Figures 4(b) and 4(c) shows separately the data at 10 and 295 K, respectively. At 10 K, the ρ_{Cu} value varies by more than a factor of 5 from 0.7 to $>4.0 \mu\Omega \text{cm}$, and the plot includes 128 data points. At 295 K, the ρ_{Cu} varies by more than a factor of 3 from $3.5 \mu\Omega \text{cm}$ to $>10 \mu\Omega \text{cm}$, and the plot includes 74 data points. The ranges of ρ_{Cu} are broader and the numbers of data points are greater than those from a single substrate, such as in Fig. 3. Establishing a detailed λ versus ρ relationship over a broad range of ρ has not been previously achieved for the studies of NLSVs.

In Fig. 4(a), The decreasing trend of λ_{Cu} as a function of ρ_{Cu} is undisputable. A fit by the Elliott-Yafet model [Eq. (3)] is shown as the dashed line and the fitted spin-flip probability is $\alpha = (5.0 \pm 0.2) \times 10^{-4}$. While the fitted curve agrees reasonably well with the trend of the experimental data in the low-resistivity range ($\rho_{Cu} < 4 \mu\Omega \text{cm}$), it deviates from the data and underestimates the experimental values of λ_{Cu} in the high-resistivity range ($\rho_{Cu} > 4 \mu\Omega \text{cm}$). Alternatively, we fit the data for 10 and 295 K separately and show

the results in Figs. 4(b) and 4(c), respectively. The fitted curves and the experimental data show better agreement as compared to the composite plot in Fig. 4(a). The fitted α values are substantially different for two temperatures: $\alpha = (5.2 \pm 0.2) \times 10^{-4}$ for 10 K and $\alpha = (2.2 \pm 0.1) \times 10^{-4}$ for 295 K, but are quite consistent with the previously obtained values for substrates No. 70-4 and No. 70-0 as shown in Fig. 3. Despite the data scattering at 295 K in Fig. 4(c), there is a slow but solid decreasing trend for λ_{Cu} as a function of ρ_{Cu} . Such a trend is consistent with the Elliott-Yafet spin-relaxation mechanism with a small α value, and it might be difficult to identify if only a subset of the data is examined as is the case in Figs. 3(b) and 3(d).

It is useful to identify the causes of the data scattering in Fig. 4. The finite widths of F_1 and F_2 electrodes lead to uncertainties of the ρ_{Cu} measurements, as previously mentioned. There are two main sources for the uncertainties for λ_{Cu} . First, the λ_{Cu} and ρ_{Cu} relationship described by Eq. (3) predicted by the Elliott-Yafet model is based on the assumption that the spin-flip probability α is fixed for any momentum scattering event. If α actually depends on the types of momentum scattering, different values of λ_{Cu} can be associated with nominally the same ρ_{Cu} value, contributing to the scattering of data. Secondly, the assumption of a fixed effective spin polarization P_e for all NLSVs on a sample substrate could lead to uncertainties in derived λ_{Cu} , because the actual P_e values might vary from device to device. Because of uncertainties in both ρ_{Cu} and λ_{Cu} , there is a clear advantage to use a large number of NLSVs on multiple substrates to examine the average trend of λ_{Cu} versus ρ_{Cu} .

The values of λ_{Cu} obtained from some NLSVs are exceptionally long. At 10 K, the fitted λ_{Cu} value varies from >2000 to ~ 500 nm, as the resistivity increases from $\rho_{Cu} \sim 0.8 \mu\Omega \text{cm}$ to $\rho_{Cu} \sim 4.0 \mu\Omega \text{cm}$. As an alternative approach to estimate, we take eight data points that exhibited the highest

values of λ_{Cu} in Fig. 4(b) and obtained the average λ_{Cu} of 2040 nm. These eight NLSVs are from three different substrates. Two of the eight devices have been measured at both temperatures and show residual resistivity ratios ~ 5 (ratio of 295 K resistivity to the 10 K resistivity). Despite the uncertainty associated with the λ_{Cu} value for a given data point, the average λ_{Cu} obtained from multiple NLSVs on various substrates can be a trustworthy estimate. At 295 K, in Fig. 4(c), the fitted λ_{Cu} varies from ~ 760 to ~ 250 nm as the ρ_{Cu} increases from ~ 3.5 to $\sim 10 \mu\Omega \text{ cm}$. The average λ_{Cu} obtained from the eight experimental data points with the largest λ_{Cu} (excluding the outlying point of $\lambda_{\text{Cu}} = 1210$ nm) is 755 nm. Summarizing the above analysis, we conclude that optimal λ_{Cu} values of $\sim 2.0 \mu\text{m}$ for 10 K and ~ 700 nm for 295 K can be achieved experimentally in mesoscopic Cu channels. For both temperatures, these optimal λ_{Cu} values are usually found in NLSVs with larger Cu channel cross sections (thickness and width between 200 and 300 nm), which often lead to larger Cu grain sizes.

IV. VARIATION OF SPIN-FLIP PROBABILITIES AND ITS ORIGIN

The spin-flip probability $\alpha_{295\text{K}} = (2.2 \pm 0.1) \times 10^{-4}$ at 295 K is substantially lower than the $\alpha_{10\text{K}} = (5.2 \pm 0.2) \times 10^{-4}$ at 10 K. There are three potential origins to account for this difference. The first scenario is that phonons have a lower spin-flip probability than defects (including crystalline defects, grain boundaries, and impurities). The momentum scattering events at 10 K are caused by defects only. At 295 K, the momentum scattering events are caused by defects and phonons. If the phonon spin-flip probability is much lower than that of the defects, the difference of α values between two temperatures can be accounted for.

The second scenario is that the spin-flip probability for surface scattering is much higher than that of the bulk scattering. At room temperature, the electron mean-free path is short and momentum scattering mainly occurs in the bulk of the Cu channel. At low temperature, the mean-free path is enhanced and more momentum scattering events occur at the surfaces of Cu channels. If the surface spin-flip probability is much higher than that of the bulk, the effective α value at low temperature would be higher than that of the room temperature.

The third scenario is that DP spin-relaxation mechanism plays a partial role. A purely DP mechanism would result in λ being independent of ρ . A purely EY mechanism results in λ decaying in the form of $1/\rho$. A combination of DP and EY dependence would give a decaying trend that is slower than $1/\rho$. Such a slower trend would result in a smaller effective α at 295 K, because the ρ_{Cu} is higher at 295 K than at 10 K. In the following, we will analyze all three scenarios and conclude that the second scenario of bulk versus surfaces is the most convincing scenario supported by the strongest evidence.

For the first scenario of phonons versus defects, we start the analysis by realizing that the difference between the momentum scattering rates at 295 and 10 K, $1/\tau_{e295\text{K}} - 1/\tau_{e10\text{K}}$, is the momentum scattering rate by phonons. Similarly, the rate of spin relaxation caused by phonons is $1/\tau_{s295\text{K}} - 1/\tau_{s10\text{K}}$. The spin-flip probability of phonons is the ratio of the phonon

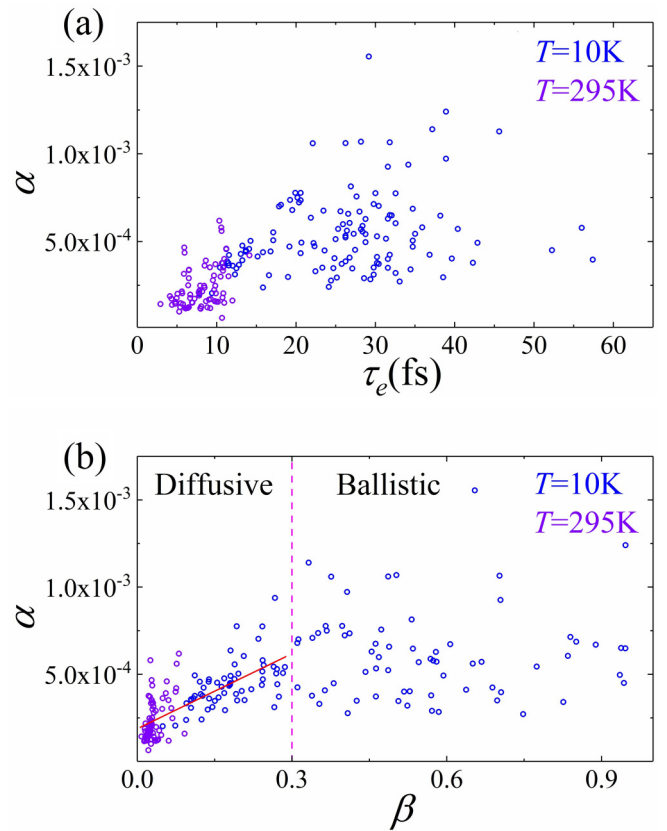


FIG. 5. (a) Spin-flip probability α versus momentum relaxation time τ_e for NLSVs at 10 K (blue) and 295 K (purple). (b) Plot of α versus β for NLSVs at 10 K (blue) and 295 K (purple). A linear fit to the data in the diffusive region ($0 < \beta < 0.3$) is shown as a solid line.

spin-relaxation rate to the phonon momentum relaxation rate:

$$\alpha_{\text{ph}} = \frac{1/\tau_{s295\text{K}} - 1/\tau_{s10\text{K}}}{1/\tau_{e295\text{K}} - 1/\tau_{e10\text{K}}} = \frac{\alpha_{295\text{K}} \rho_{\text{Cu}295\text{K}} - \alpha_{10\text{K}} \rho_{\text{Cu}10\text{K}}}{\rho_{\text{Cu}295\text{K}} - \rho_{\text{Cu}10\text{K}}}. \quad (4)$$

Note that here we used relationships $1/\tau_{s10\text{K}} = \alpha_{10\text{K}}/\tau_{e10\text{K}}$, $1/\tau_{s295\text{K}} = \alpha_{295\text{K}}/\tau_{e295\text{K}}$, and $\tau_e = m/(\rho_{\text{Cu}} n e^2)$. Using average ρ_{Cu} values of $5.73 \mu\Omega \text{ cm}$ at 295 K and $1.92 \mu\Omega \text{ cm}$ at 10 K, we estimate $\alpha_{\text{ph}} = 6.9 \times 10^{-5}$, which is much lower than the 5.2×10^{-4} for defects. However, a low value of $\alpha_{\text{ph}} < 1 \times 10^{-4}$ is not really supported by any previous theoretical or experimental work [20,21].

For the second scenario of surfaces versus bulk, we intend to correlate α values with a parameter that represents the probability of surface scattering. The simplest parameter for this purpose is τ_e . A higher τ_e implies a longer mean-free path ($v_F \cdot \tau_e$) and a higher probability of reaching surfaces. We calculate an α [from the λ_{Cu} and ρ_{Cu} using Eq. (3)] and a τ_e (from ρ_{Cu}) for each given NLSV. In Fig. 5(a), these α values for all NLSVs at 10 and 295 K are plotted as a function of τ_e . The variation of α in Fig. 5(a) is substantial, ranging from $< 1.0 \times 10^{-4}$ to $> 1.0 \times 10^{-3}$. However, the distribution of data points on the plot forms a surprising fan shape. The highest available α values decrease clearly as τ_e decreases. The average α values also decrease as τ_e decreases. As τ_e approaches zero, α values converge to a low

value of $\alpha \approx 2 \times 10^{-4}$. This plot gives the first indication of a systematic trend.

However, τ_e alone is not sufficient to characterize the surface scattering probabilities, which are also influenced by the dimensions of the Cu channels. Therefore, we define a parameter: surface scattering probability $\beta = \tau_e/\tau_{e\text{-surf}}$, where $\tau_{e\text{-surf}}$ is the average time for an electron to experience scattering from any surface. In the following, we use a simple model to derive an expression for $\tau_{e\text{-surf}}$. In a complete diffusive regime ($\beta \rightarrow 0$), the elapsed time for an electron to diffuse over a displacement d in three-dimensional space is given by $\tau_d = d^2/(6D)$, where D is the diffusion constant. The diffusion time can be derived by a random-walk model and takes the forms of $\tau_d = d^2/(2D)$, $\tau_d = d^2/(4D)$, and $\tau_d = d^2/(6D)$ for one, two, and three dimensions, respectively.

Consider an electron at the center of the Cu channel. To reach the side surfaces of the channel it has to diffuse over a distance $w/2$ in directions that are perpendicular to the side surfaces, where w is the width of the channel. The elapsed time for diffusion over a distance of $w/2$ in any direction is $w^2/(24D)$. However, considering the three possible dimensions to diffuse, the time to reach either of the two side surfaces should increase by a factor of 3: $\tau_1 = w^2/(8D)$. Similarly, the time to reach the top or bottom surfaces of the channel is $\tau_2 = t^2/(8D)$, where t is the thickness of the channel. Then the rate of scattering from any surfaces is

$$\frac{1}{\tau_{e\text{-surf}}} = \frac{1}{\tau_1} + \frac{1}{\tau_2} = 8D \left(\frac{1}{w^2} + \frac{1}{t^2} \right). \quad (5)$$

For each NLSV, $\tau_{e\text{-surf}}$ can be calculated from its dimensions (w and t) and the resistivity ρ_{Cu} (related to D). Then it can be used to calculate β , which represents the probability of surface scattering for each momentum scattering event.

Figure 5(b) shows the plot of α versus β for 10 and 295 K. The β values are broadly distributed from < 0.1 to nearly 1. Here we can divide the data into two regions: the diffusive transport region of $0 < \beta < 0.3$ and the nearly ballistic transport region of $0.3 < \beta < 1$. The choice of $\beta = 0.3$ as the threshold value is empirical. A systematic trend can be seen in the region of $0 < \beta < 0.3$, where α_s increases uniformly and linearly as β increases. A linear fit to the data, shown in Fig. 5(b), yields a positive slope and a positive intercept on the vertical axis. For $\beta > 0.3$, there is no obvious dependence of α as a function of β . We note that Eq. (5) is based on transport in the diffusive regime, which implies a small β value. For larger β values, the transport is nearly ballistic and therefore the derived β values may not correlate well with the actual probability of surface scattering.

The linear increase of α upon β is consistent with and strongly supports this scenario of surface versus bulk. When $\beta \rightarrow 0$, the scattering events occur predominantly in the bulk, and the α value in this limit (intercept with vertical axis) represents the bulk spin-flip probability. As β increases, the electron has a higher probability of experiencing surface scattering, and the slope of increase for the α versus β plot reflects the difference between the surface and bulk spin-flip probabilities. The quantitative relationship between α and β is derived to be

$$\alpha = \alpha_{\text{bulk}} + (\alpha_{\text{surf}} - \alpha_{\text{bulk}})\beta, \quad (6)$$

where α_{bulk} and α_{surf} are spin-flip probabilities for momentum scattering in the bulk and at the surfaces, respectively. In deriving Eq. (6), we used relations such as $1/\tau_s = \alpha_{\text{bulk}}/\tau_{e\text{-bulk}} + \alpha_{\text{surf}}/\tau_{e\text{-surf}}$ and $1/\tau_e = 1/\tau_{e\text{-bulk}} + 1/\tau_{e\text{-surf}}$ and the definition of α and β given earlier. Here $\tau_{e\text{-bulk}}$ is momentum relaxation time related to bulk scattering. Indeed, Eq. (6) indicates that the α versus β curve is linear with a vertical intercept of α_{bulk} and a slope of $\alpha_{\text{surf}} - \alpha_{\text{bulk}}$.

From the vertical intercept and the slope of the fitted straight line in Fig. 5(b), we obtain $\alpha_{\text{bulk}} = (1.9 \pm 0.2) \times 10^{-4}$ and $(\alpha_{\text{surf}} - \alpha_{\text{bulk}}) = (1.4 \pm 0.1) \times 10^{-3}$, respectively. Therefore, the surface spin-flip probability is $\alpha_{\text{surf}} = (1.6 \pm 0.2) \times 10^{-3}$, which is > 8 times of the value of α_{bulk} . Previously a large value of α_{surf} was suggested to explain an unusual temperature dependence of spin signal in NLSVs [22–24], but later O’Brien *et al.* attributed the phenomenon to Kondo effects instead [25]. More recently, Zhou *et al.* [11] reported anisotropic spin relaxation in Cu channels of NLSVs and attributed the effects to surface spin-orbit effects of Rashba type, which would induce large α_{surf} values on the surfaces of mesoscopic Cu channels.

The third scenario of possible DP contribution is tempting to consider. A combined model of EY and DP mechanisms would give a decaying trend of λ_{Cu} slower than $1/\rho_{\text{Cu}}$. The fitting of the data in Fig. 4(a) would be improved and the difference in α between 10 and 295 K can be possibly accounted for. However, the second scenario of a large α_{surf} also implies a slowly decaying λ_{Cu} versus ρ_{Cu} curve. The fitting of λ_{Cu} versus ρ_{Cu} can be improved by taking into account surface scattering, as will be shown in the next section. In addition, the separate sets of data at 10 and 295 K, in Figs. 4(b) and 4(c), respectively, can be fitted reasonably well by the EY model alone. This casts doubt on a significant contribution of DP mechanism. On a cautionary note, however, we would not totally dismiss the presence of the DP mechanism.

For the three possible scenarios, the second scenario of bulk versus surface is supported by the strongest evidence and therefore is the most convincing one. The unequivocal linear relation of α versus β in Fig. 5(b) demonstrates that there is indeed a substantial difference between bulk and surface spin-flip probabilities. At this point, we conclude that the spin-relaxation mechanism in mesoscopic Cu channels can be described well by the EY model. However, the spin-flip probability of the surface is much larger than that of the bulk.

The difference of α values between 295 and 10 K can be accounted for by this scenario as well. The value of $\alpha = (2.2 \pm 0.1) \times 10^{-4}$ at 295 K, obtained from the λ_{Cu} versus ρ_{Cu} plot in Fig. 4(c), is close to $\alpha_{\text{bulk}} = (1.9 \pm 0.2) \times 10^{-4}$. At 295 K, the mean-free paths of the electrons are much smaller than the dimensions of the Cu channel and the electrical transport is dominated by bulk scattering. At 10 K, the mean-free paths are longer and surface scattering probability is higher, leading to a higher average value of $\alpha = (5.2 \pm 0.2) \times 10^{-4}$ as obtained from the λ_{Cu} versus ρ_{Cu} plot in Fig. 4(b).

One point of discussion is how the surface momentum scattering would influence the values of resistivity. Experiments show that momentum scattering events from surfaces of mesoscopic metallic wires are nonspecular, meaning that the momentum direction is completely randomized after scattering [26]. Therefore, surface scattering

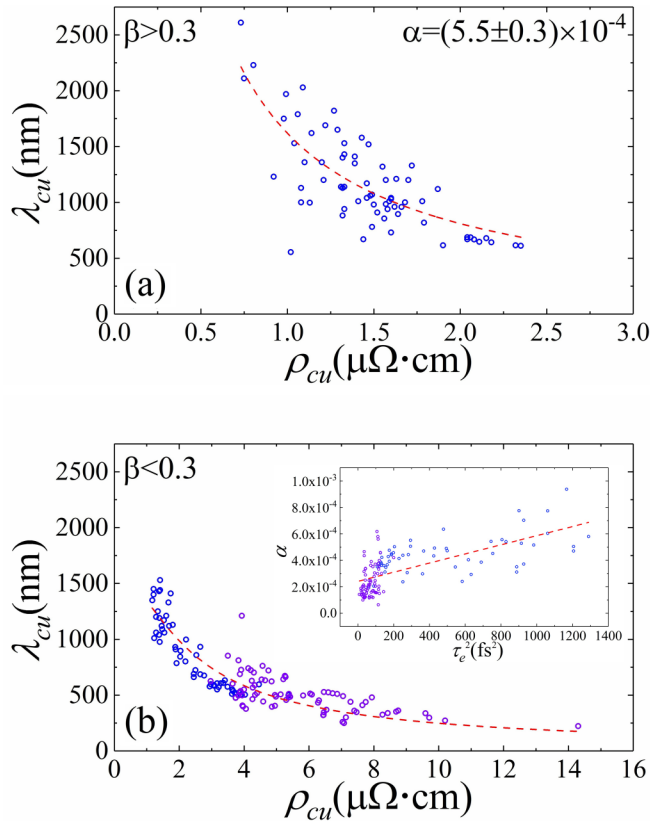


FIG. 6. (a) Plot of λ_{Cu} versus ρ_{Cu} for NLSVs with nearly ballistic transport in Cu channels ($\beta > 0.3$). The data are fitted by Eq. (3) with a fixed α . (b) Plot of λ_{Cu} versus ρ_{Cu} for NLSVs with diffusive transport ($\beta < 0.3$). The inset shows the α versus τ_e^2 plot and a linear fit. A λ_{Cu} versus ρ_{Cu} curve is generated from the fit and shown as the dashed line in the main panel of (b). Data at 10 and 295 K are shown as blue and purple colors, respectively.

contributes to the resistivity in the same manner as bulk scattering.

V. REVISITING λ_{Cu} VERSUS ρ_{Cu} RELATIONSHIP

The fitting of λ_{Cu} versus ρ_{Cu} relationship for the entire data set in Fig. 4(a) is not satisfactory because the fitting assumed a fixed α , which is not the case in reality. In this section, we attempt to fit the λ_{Cu} versus ρ_{Cu} relationship in a better manner by taking into account the varying α values. We now group the data according to β instead of temperatures. In Fig. 6, we divide all data (10 and 295 K) into two groups: one for $\beta > 0.3$ (nearly ballistic devices) and the other for $\beta < 0.3$ (diffusive devices). Data in the former group are all from 10 K, but the latter group contains data from both 10 and 295 K. Plots of λ_{Cu} versus ρ_{Cu} are shown for $\beta > 0.3$ and $\beta < 0.3$ in Figs. 6(a) and 6(b), respectively. The fitting for the data in Fig. 6(a) by the Elliott-Yafet model yields $\alpha = (5.5 \pm 0.3) \times 10^{-4}$, a value that is between α_{bulk} and α_{surf} . The

bulk momentum scattering in the channels is not negligible, because the channel length is still substantially longer than the mean-free path. The decreasing trend of the experimental data in Fig. 6(a) is pronounced and is described well by the fitted curve.

For diffusive devices with $\beta < 0.3$, we attempt a different fitting method to reflect the subtle variations of α values. In the inset of Fig. 6(b), we plot the α as a function of τ_e^2 for these devices. An increase of α with an increasing τ_e^2 is obvious. If all devices have identical Cu channel cross sections, the α versus τ_e^2 plot would be equivalent to the α versus β plot, as can be easily proven by using Eq. (5) and the definition of β . Interestingly, even with the variation in Cu cross sections, this α versus τ_e^2 plot in the diffusive region is qualitatively similar to the α versus β in Fig. 5(b). We fit the experimental data of α versus τ_e^2 (for $\beta < 0.3$) with a straight line, as shown in the inset of Fig. 6(b). From the fitted α versus τ_e^2 relation, we calculate a relationship between λ_{Cu} and ρ_{Cu} , which is shown as the dashed line in the main panel of Fig. 6(b). This generated dashed line describes the experimental data in Fig. 6(b) reasonably well over a broad range of ρ_{Cu} from 1 to $> 10 \mu\Omega \text{ cm}$. It is a clear improvement compared to the fitting in Fig. 4(a) with a fixed α value.

VI. CONCLUSIONS

In conclusion, a large number of nonlocal spin valves are used to establish a relationship between spin-relaxation length λ_{Cu} and resistivity ρ_{Cu} for mesoscopic Cu channels over a broad range of ρ_{Cu} . By quantifying the relationship with various approaches, we conclude that the spin relaxation can be described well by the Elliott-Yafet model. However, the spin-flip probabilities for bulk and surface scattering are $\alpha_{\text{bulk}} = (1.9 \pm 0.2) \times 10^{-4}$ and $\alpha_{\text{surf}} = (1.6 \pm 0.2) \times 10^{-3}$, respectively, differing by a factor of > 8 . This also explains the apparent difference between the average spin-flip probability of $\alpha_{10 \text{ K}} = (5.2 \pm 0.2) \times 10^{-4}$ at 10 K and that of $\alpha_{295 \text{ K}} = (2.2 \pm 0.1) \times 10^{-4}$ at 295 K. In devices with larger Cu channel cross sections (200 to 300 nm in width and thickness), we find low ρ_{Cu} , large residual resistivity ratio, and long λ_{Cu} ($\sim 2.0 \mu\text{m}$ at 10 K and $\sim 700 \text{ nm}$ at 295 K). These experimentally achievable optimal spin-relaxation lengths provide encouraging prospects for spin transport in mesoscopic non-magnetic metals.

ACKNOWLEDGMENTS

Work at Fudan University was supported by the National Key Basic Research Program of China (Grant No. 2015CB921401), National Key Research and Development Program of China (Grant No. 2016YFA0300703), National Natural Science Foundation of China (Grants No. 11474066, No. 11734006, and No. 11434003), and the Program of Shanghai Academic Research Leader (Grant No. 17XD1400400). Y.L. was supported by National Natural Science Foundation of China (Grant No. 11604066).

[1] Y. Yafet, *Phys. Lett. A* **98**, 287 (1983).
 [2] R. J. Elliott, *Phys. Rev.* **96**, 266 (1954).

[3] M. I. Dyakonov and V. I. Perel, *Sov. Phys. Solid State, USSR* **13**, 3023 (1972).

- [4] M. Johnson and R. H. Silsbee, *Phys. Rev. Lett.* **55**, 1790 (1985).
- [5] F. J. Jedema, A. T. Filip, and B. J. van Wees, *Nature (London)* **410**, 345 (2001).
- [6] F. J. Jedema, H. B. Heersche, A. T. Filip, J. J. A. Baselmans, and B. J. van Wees, *Nature (London)* **416**, 713 (2002).
- [7] S. O. Valenzuela and M. Tinkham, *Appl. Phys. Lett.* **85**, 5914 (2004).
- [8] T. Kimura, J. Hamrle, and Y. Otani, *Phys. Rev. B* **72**, 014461 (2005).
- [9] Y. Ji, A. Hoffmann, J. S. Jiang, and S. D. Bader, *Appl. Phys. Lett.* **85**, 6218 (2004).
- [10] R. Godfrey and M. Johnson, *Phys. Rev. Lett.* **96**, 136601 (2006).
- [11] C. Zhou, F. Kandaz, Y. J. Cai, C. Qin, M. W. Jia, Z. Yuan, Y. Z. Wu, and Y. Ji, *Phys. Rev. B* **96**, 094413 (2017).
- [12] Y. Ji, A. Hoffmann, J. E. Pearson, and S. D. Bader, *Appl. Phys. Lett.* **88**, 052509 (2006).
- [13] X. J. Wang, H. Zou, L. E. Ocola, and Y. Ji, *Appl. Phys. Lett.* **95**, 022519 (2009).
- [14] Y. J. Cai, Y. M. Luo, C. Zhou, C. Qin, S. H. Chen, Y. Z. Wu, and Y. Ji, *J. Phys. D: Appl. Phys.* **49**, 185003 (2016).
- [15] M. Johnson, *Phys. Rev. Lett.* **70**, 2142 (1993).
- [16] S. Takahashi and S. Maekawa, *Phys. Rev. B* **67**, 052409 (2003).
- [17] *Solid State Physics*, edited by N. W. Ashcroft and N.D. Mermin (Saunders College Publishing, Philadelphia, 1976).
- [18] F. J. Jedema, M. S. Nijboer, A. T. Filip, and B. J. van Wees, *Phys. Rev. B* **67**, 085319 (2003).
- [19] V. Palenskis, *AIP Adv.* **4**, 047119 (2014).
- [20] F. Beuneu and P. Monod, *Phys. Rev. B* **13**, 3424 (1976).
- [21] E. Villamor, M. Isasa, L. E. Hueso, and F. Casanova, *Phys. Rev. B* **87**, 094417 (2013).
- [22] T. Kimura, T. Sato, and Y. Otani, *Phys. Rev. Lett.* **100**, 066602 (2008).
- [23] G. Mihajlovic, J. E. Pearson, S. D. Bader, and A. Hoffmann, *Phys. Rev. Lett.* **104**, 237202 (2010).
- [24] H. Zou and Y. Ji, *Appl. Phys. Lett.* **101**, 082401 (2012).
- [25] L. O'Brien, M. J. Erickson, D. Spivak, H. Ambaye, R. J. Goyette, V. Lauter, P. A. Crowell, and C. Leighton, *Nat. Commun.* **5**, 3927 (2014).
- [26] Q. J. Huang, C. M. Lilley, and M. Bode, *Appl. Phys. Lett.* **95**, 103112 (2009).